Reduction and Re-oxidation Behavior of Calcium Iron Phosphate, $Ca_9Fe(PO_4)_7$

B. I. Lazoryak,*,† A. A. Belik,† R. N. Kotov,‡ I. A. Leonidov,§ E. B. Mitberg,§ V. V. Karelina,§ D. G. Kellerman,§ S. Yu. Stefanovich,‡ and A. K. Avetisov‡

Department of Chemistry, Moscow State University, 119899 Moscow, Russia, State Scientific Center of Russian Federation, Karpov Institute of Physical Chemistry, 103063, Moscow, Russia, and Institute of Solid State Chemistry, Ural Branch of RAS, Pervomayskaia 91, GSP-145, 620219 Yekaterinburg, Russia

Received September 13, 2001. Revised Manuscript Received October 3, 2002

Reduction (in H_2) and re-oxidation (in air) behavior of $Ca_9Fe(PO_4)_7$ was studied by X-ray powder diffraction, Mössbauer spectroscopy, thermogravimetry, hydrogen absorption, electrical conductivity, and magnetic-susceptibility measurements. The β-$Ca_3(PO_4)_2$-like framework of $Ca_9Fe(PO_4)_7$ was stable in 100% H_2 up to 820 K. In the temperature range from 680 to 820 K, reversible redox reactions occurred without changing the stoichiometry of oxygen and phosphorus atoms and destroying the structure. The reduction process in $Ca_9Fe(PO_4)_7$ included the change of the oxidation state of Fe atoms and incorporation of hydrogen atoms into the structure to form $Ca_9FeH_x(PO_4)_7$ ($0 < x \leq 1$). Above 820 K, treatment in 100% H_2 was accompanied by loss in mass, partial destruction of the structure, and appearance of FeP and Fe_2P phases. Re-oxidation studies in air showed that samples partially lost phosphorus atoms during reduction above 820 K. Behavior of $Ca_9Fe(PO_4)_7$ under a reduction atmosphere depended on H_2 concentration and temperature. At low H_2 concentration, the sample destruction started from ca. 870 K and proceeded with maintaining the oxidation state of Fe, releasing H_2O, and forming a β-$Ca_3(PO_4)_2$-like phase and β-$Ca_2P_2O_7$. In this case, iron phosphides appeared above ca. 1200 K.

Introduction

Phosphates containing transition metals are of interest for their numerous practical applications. For example, they have been extensively studied as catalysts,[1−5] cathode materials for Li-ion batteries,[6] materials intermediators for two-stage oxidation of H_2,[7,8] materials for cleaning gas mixtures from H_2,[9,10] and sensors.[11]

A large number of investigations have been carried out to study physicochemical and catalytic properties of iron phosphates.[12] For example, $FePO_4$ has catalytic activity in oxidative dehydrogenation reactions.[13] Its behavior in H_2 was studied by Gadgil and Kulshreshtha.[14]

Phosphates containing Ni,[1] Co,[3] and Cd[4] atoms and possessing the β-$Ca_3(PO_4)_2$-type[15] structure have catalytic activity in dehydrogenation reactions, for example, for converting *n*-butenes to butadience and for oxydehydrogenating lower aliphatic alkanes and alkenes to dienes.[2] Catalytic activity in solid solutions $Ca_{3-x}Ni_x(PO_4)_2$ was suggested to be caused by the presence of Ni^{3+} ions.[1] The possibility of formation of Co^{3+} ions in calcium cobalt phosphates has been shown in the literature.[16] Catalytic properties of $Ca_{10.5-x}Cu_x(PO_4)_7$ and $Ca_{10-x/2}Na_xCu_{0.5}(PO_4)_7$ ($0 \leq x \leq 1$) were studied in butan-2-ol dehydrogenation.[5] Maximum activity was found for

* To whom correspondence should be addressed. Tel.: 7-095-939-21-38. Fax: 7-095-938-24-57. E-mail: lazoryak@tech.chem.msu.ru.
† Moscow State University.
‡ Karpov Institute of Physical Chemistry.
§ Institute of Solid State Chemistry.

(1) (a) Attali, S.; Vigouroux, B.; Lenzi, M.; Perscia, J. *J. Catal.* **1980**, *63*, 496. (b) Legrouri, A.; Lenzi, J.; Lenzi, M. *J. Therm. Anal.* **1993**, *39*, 1321.
(2) (a) Vrieland, G. E. (The Dow Chemical Co.) US Patent 3,935,-126, 1974. (b) Krabbenhoft, H. O. (General Electric Co.) US Patent 4,346,249, 1981. (c) Krabbenhoft, H. O. (General Electric Co.) US Patent 4,366,089, 1981. (d) Strickler, G. R. (The Dow Chemical Co.) US Patent 4,471,146, 1983. (e) Lee, S. J.; Jun, J. H.; Lee, S.-H.; Yoon, K. J.; Lim, T. H.; Nam, S.-W.; Hong, S.-A. *Appl. Catal. A* **2002**, *230*, 61.
(3) (a) Legrouri, A.; Romdhane, S. S.; Lenzi, J.; Lenzi, M.; Bonel, G. *J. Mater. Sci.* **1996**, *31*, 2469. (b) Legrouri, A.; Lenzi, J.; Lenzi, M. *Mater. Chem. Phys.* **1994**, *38*, 94.
(4) Attali, S.; Lenzi, J.; Lenzi, M. *Bull. Chem. Soc. France* **1981**, I-135.
(5) Benarafa, A.; Kacimi, M.; Coudurier, G.; Ziyad, M. *Appl. Catal. A* **2000**, *196*, 25.
(6) (a) Alvarez-Vega, M.; Garcia-Moreno, O.; Garcia-Alvardo, F.; Garcia-Jaca, J.; Gallardo-Amores, J. M.; Sanjuan, M. L.; Amador, U. *Chem. Mater.* **2001**, *13*, 1570. (b) Yang, S.; Zavalij, P. Y.; Whittingham M. S. *Electrochem. Commun.* **2001**, *3*, 505.
(7) Safonov, M. S.; Lazoryak, B. I.; Pozharskii, S. B.; Dashkov, S. B. *Dokl. Acad. Nauk.* **1994**, *338*, 633. (*Eng. Transl.* **1995**, *345*, 849.)
(8) Lazoryak, B. I.; Morozov, V. A.; Safonov, M. S.; Khasanov, S. S. *Mater. Res. Bull.* **1995**, *30*, 1269.
(9) Lazoryak, B. I.; Morozov, V. A.; Zhdanova, A. N. RF Patent 2081820, 1995.
(10) Lazoryak, B. I.; Zhdanova, A. N.; Morozov, V. A.; Khan, N. RF Patent 2129983, 1999.
(11) Lazoryak, B. I. In *Fundamental Study of New Materials and Processes in the Substance* (in Russian); Moscow State University Press: Moscow, 1994; p 54.
(12) (a) Millet, J.-M. M. *Catal. Rev.* **1998**, *40*, 1. (b) Bonnet, P.; Millet, J.-M. M.; Leclercq, C.; Vedrine, J. C. *J. Catal.* **1996**, *158*, 128.
(13) Miller, J. E.; Gonzales, M. M.; Evans, L.; Sault, A. G.; Zhang, C.; Rao, R.; Whitwell, G.; Maiti, A.; King-Smith D. *Appl. Catal. A* **2002**, *231*, 281.
(14) Gadgil, M. M.; Kulshreshtha, S. K. *J. Solid State Chem.* **1994**, *111*, 357.
(15) Dickens, B.; Schroeder, L. W.; Brown, W. E. *J. Solid State Chem.* **1974**, *10*, 232.
(16) Belik, A. A.; Morozov, V. A.; Khasanov, S. S.; Lazoryak, B. I. *Mater. Res. Bull.* **1998**, *33*, 987.

10.1021/cm010851l CCC: $25.00
Published on Web 01/11/2003

compositions at the Cu-rich boundary of solid solutions with the β-$Ca_3(PO_4)_2$-like structure.

β-$Ca_3(PO_4)_2$-like compounds containing Fe and Ce atoms have not been studied yet as catalysts. Fe, Cu, and Ce atoms can be reduced and oxidized in softer conditions (giving Fe^{3+}/Fe^{2+}, Cu^{2+}/Cu^{+}, and Ce^{4+}/Ce^{3+} redox couples) than Co and Ni atoms. In $Ca_9Fe(PO_4)_7$,[8,17,18] $Ca_{9.5}Cu(PO_4)_7$,[5,19] $Ca_{3-x}Ce_{0.5x}(PO_4)_2$ ($0 \le x \le 0.29$),[20] and $Ca_9Na_{1.5}Fe_{0.5}(PO_4)_7$,[21] redox reactions occur without destroying fundamental structures according to the following reactions exemplified for $Ca_9Fe(PO_4)_7$:[17,22]

$$2Ca_9Fe^{3+}(PO_4)_7 + H_2 = 2Ca_9Fe^{2+}H(PO_4)_7 \quad (1)$$

$$4Ca_9Fe^{2+}H(PO_4)_7 + O_2 = 4Ca_9Fe^{3+}(PO_4)_7 + 2H_2O \quad (2)$$

However, mechanisms of these reactions and stability of these compounds in H_2 at high temperatures have not been studied enough. Such data are important for potential applications of these phosphates as catalysts, materials intermediators for two-stage oxidation of H_2, materials for cleaning gas mixtures from H_2, and sensors. We have recently clarified the structural mechanisms of reactions 1 and 2 comparing structure parameters of $Ca_9Fe(PO_4)_7$[17] and $Ca_9FeD(PO_4)_7$.[22] In this paper, we have studied reduction (re-oxidation) behavior of $Ca_9Fe(PO_4)_7$ ($Ca_9FeH_x(PO_4)_7$) in H_2 (air) at different temperatures and gas concentrations.

Experimental Section

Synthesis. $Ca_9Fe(PO_4)_7$ was synthesized from stoichiometric mixtures of Fe_2O_3, $Ca_2P_2O_7$, and $CaCO_3$ by the solid-state method at 1300 K for 150 h (ground every 30 h) in alumina crucibles. All the starting components were of analytical grade. As-synthesized samples, s-$Ca_9Fe(PO_4)_7$ (ICDD PDF #45-338), were light red and contained a very small amount of α-Fe_2O_3 (ICDD PDF #84-311).

X-ray Powder Diffraction (XRD) Experiments. XRD measurements were performed at room temperature (RT) on a SIEMENS D500 Bragg−Brentano-type powder diffractometer operated at 30 kV and 30 mA. The diffractometer was equipped with an incident-beam quartz-monochromator to obtain Cu Kα_1 radiation ($\lambda = 1.5406$ Å) and a BRAUN position-sensitive detector (PSD). Si (NIST Standard Reference Material 640b) was used as an external standard material for diffraction angles. XRD data were collected in a 2θ range from 10° to 60° with a step interval of 0.02°. Effective counting time per step was 1 min; that is, during this time each 2θ angle was within PSD. To detect α-Fe_2O_3 in s-$Ca_9Fe(PO_4)_7$, we used an effective counting time of ca. 1.5 h/step (with PSD) in a 2θ range from 31° to 37°. With the usually used counting time, we could not detect α-Fe_2O_3 by XRD because of its small amount and because the two strongest reflections of α-Fe_2O_3 with $d = 2.677$ Å ($I/I_1 = 100\%$) and $d = 2.501$ Å ($I/I_1 = 75\%$) almost coincide with reflections of s-$Ca_9Fe(PO_4)_7$. We used the Rietveld method[23] to separate reflections of the two phases. Lattice parameters given throughout this paper were refined by the Rietveld method[23] with RIETAN-97.[24] Mass fractions of phases were calculated from scale factors refined by Rietveld analyses of the XRD data with RIETAN-97.

Magnetic-Susceptibility Measurements and Mössbauer Spectroscopy. Magnetic susceptibilities, χ, were measured with a Faraday-type magnetometer between 300 and 1000 K in air. ^{57}Fe Mössbauer spectra were recorded at RT using a constant-acceleration Mössbauer spectrometer coupled with a multichannel analyzer and a ^{57}Co/Cr (or ^{57}Co/Rh) source kept at RT. All the isomer shifts, δ, were determined with reference to α-Fe. We used samples with the natural content of ^{57}Fe (2.2%) and containing 14% of ^{57}Fe.

Electrical-Conductivity Measurements. To measure the dc electrical conductivities, σ, we used samples in the form of pellets 4−5 mm in length and 5−6 mm in diameter. They were pelletized by pressing at 1 kbar and sintering at 1300 K for 3 h (cooling rate: 4 K/min). The densities of the resultant pellets rose to 90% of the theoretical density. Pt electrodes were put on flat surfaces of the pellets. The impedance spectroscopy method performed with a Solatron 1260 frequency response analyzer in a frequency range from 1 to 10^6 Hz was used to determine the σ values.

Thermogravimetry (TG). Changes in mass were registered with Sartorius scales in quartz reactors in flowing gases, 100% H_2 or air, with a gas-flow rate of ca. 10 dm^3/h, a heating rate of ca. 4 K/min, and sample weights of 500−800 mg and with a SETARAM TG-DTA-92 instrument in flowing gases, 5% H_2 + 95% N_2 or air, with sample weights of ca. 100 mg.

Hydrogen-Absorption Measurements. H_2 absorption curves were obtained in a setup including a quartz-tube reactor and a water manometer. Samples were placed in the reactor, heated in an Ar flow up to the temperature required, and kept at this temperature for ca. 2 h. After that, the Ar flow was terminated, the reactor was partially evacuated, and then a portion of H_2 was injected through a thick-walled rubber tube by a syringe. The temperature was controlled by a Pt−Pt/Rh thermocouple with an accuracy of ±0.5 K. The pressure in the reactor was monitored by the water manometer. Initial and final H_2 concentrations in the reactor were ca. 15% and 10%, respectively.

We also carried out two experiments when the setup was filled by H_2. We changed the temperature in the reactor stepwise and measured H_2 pressure, $p(H_2)$, after 30 min. In the first experiment, the reactor did not contain s-$Ca_9Fe(PO_4)_7$. In the second one, a quartz crucible with s-$Ca_9Fe(PO_4)_7$ was placed in the reactor.

Results and Discussion

Reduction of $Ca_9Fe(PO_4)_7$ in 100% H_2. Figure 1 displays changes in mass of four different samples s-$Ca_9Fe(PO_4)_7$ heated in a flow of H_2. Each sample was heated from RT to a certain temperature, 750 K (sample I), 910 K (sample II), 1020 K (sample III), and 1220 K (sample IV), with the constant heating rate and then cooled in the H_2 flow with a furnace. After cooling, samples I−IV were examined by XRD (Figure 2b−e) and Mössbauer spectroscopy (Figure 3e−g and Table 1). The TG curves of s-$Ca_9Fe(PO_4)_7$ are divided into four temperature ranges (Figure 1): the first (300−630 K) and third (720−820 K) ranges with no change in mass and the second (630−720 K) and fourth (>820 K) temperature ranges where loss in mass was observed.

Loss in mass of ca. 0.1% for s-$Ca_9Fe(PO_4)_7$ (Figure 1) at 630−720 K was probably associated with the presence of α-Fe_2O_3. Mass fraction of α-Fe_2O_3 estimated from the TG data was ca. 0.4% (the estimation was

(17) Lazoryak, B. I.; Morozov, V. A.; Belik, A. A.; Khasanov, S. S.; Shekhtman, V. Sh. *J. Solid State Chem*. **1996**, *122*, 15.
(18) Benarafa, A.; Kacimi, M.; Gharbage, S.; Millet, J.-M. M.; Ziyad, M. *Mater. Res. Bull.* **2000**, *35*, 2047.
(19) Lazoryak, B. I.; Khan, N.; Morozov, V. A.; Belik, A. A.; Khasanov, S. S. *J. Solid State Chem*. **1999**, *145*, 345.
(20) Lazoryak, B. I.; Salmon, R.; Parent, C.; Hagenmuller, P.; Vieting, B. N.; Yaroslavtsev, A. B. *Vestn. Mosk. Univ. Ser. 2. Khim*. **1990**, *31*, 406.
(21) Strunenkova, T. V.; Morozov, V. A.; Khasanov, S. S.; Pokholok, K. V.; Zhdanova, A. N.; Lazoryak, B. I. *Crystallogr. Rep*. **1997**, *42*, 64.
(22) Belik, A. A.; Izumi, F.; Stefanovich, S. Yu.; Lazoryak, B. I.; Oikawa K. *Chem. Mater*. **2002**, *14*, 3937.
(23) Rietveld, H. M. *J. Appl. Crystallogr*. **1969**, *2*, 65.
(24) Izumi, F. In *The Rietveld Method*, Oxford University Press: New York, 1993; Chapter 13.

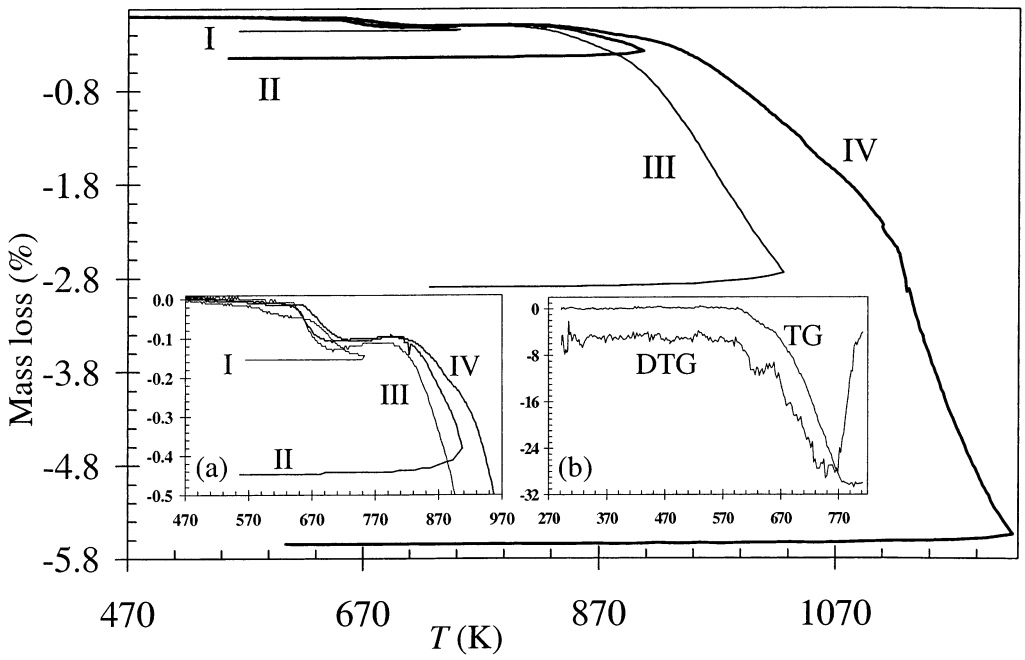

Figure 1. TG curves for s-$Ca_9Fe(PO_4)_7$ in 100% H_2. Samples I, II, III, and IV were heated from RT to 750, 910, 1020, and 1220 K, respectively. Inset (a) shows loss in mass from 0% to 0.5%. Inset (b) presents the TG and DTG curves for α-Fe_2O_3 in 100% H_2.

based on the assumption (see Figure 1b) of reducing Fe_2O_3 to Fe). Figure 1b presents a TG curve for α-Fe_2O_3 under the same conditions as that for s-$Ca_9Fe(PO_4)_7$. Loss in mass for α-Fe_2O_3 was observed in the temperature range from 600 to 770 K. Loss in mass of ca. 0.1% for s-$Ca_9Fe(PO_4)_7$ was detected almost in the same temperature range.

Dramatic loss in mass for s-$Ca_9Fe(PO_4)_7$ started above 820 K (Figure 1). Sample II lost ca. 0.45% of its mass and was light gray. However, the Mössbauer spectrum of sample II consisted of two doublets with $\delta \approx 1.20$ mm/s (Figure 3e) characteristic of Fe^{2+} ions. XRD showed sample II to be monophasic and contain only a β-$Ca_3(PO_4)_2$-like phase (Figure 2c) with lattice parameters close to those of $Ca_9FeH(PO_4)_7$ ($a = 10.3689(5)$ Å and $c = 37.128(2)$ Å; see below).

Sample III lost ca. 2.9% of its mass (Figures 1 and 4a) and was dark gray. The Mössbauer spectrum of sample III exhibited ca. 13% of Fe atoms with $\delta \approx 0.13$ mm/s (Figure 3f), which may be assigned to FeP (see below, sample IV).[25] But XRD showed only the presence of a β-$Ca_3(PO_4)_2$-like phase with lattice parameters close to those of $Ca_9FeH(PO_4)_7$ (Figure 2d). FeP in sample III was probably amorphous. The increase in mass of ca. 1.0% during re-oxidation in air (Figure 4b) was less than the loss in mass. This fact suggested that sample III lost P atoms during treatment in 100% H_2.

Using the combination of experimental facts described below, the following scheme of reduction in 100% H_2 can be given for sample IV, which was black:

$$Ca_9Fe^{3+}(PO_4)_7 \xrightarrow{H_2} 3.066Ca_{2.935}Fe^{2+}_{0.065}(PO_4)_2 + 0.560FeP + 0.120Fe_2P + \text{“}0.188P + 3.472H_2O\text{”}\uparrow. \quad (3)$$

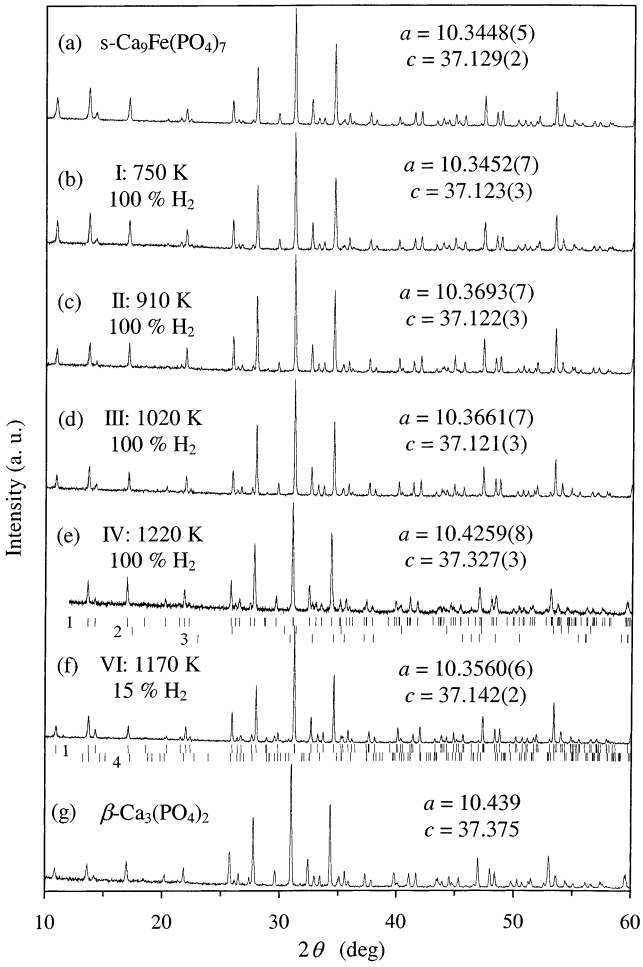

Figure 2. XRD patterns of s-$Ca_9Fe(PO_4)_7$ (a), samples I (b), II (c), III (d), and IV (e) (see Figure 1), sample VI (f) (see text), and β-$Ca_3(PO_4)_2$ (g). Lattice parameters (Å) with estimated standard deviations for β-$Ca_3(PO_4)_2$-like phases are given on the figure. Bragg reflections of β-$Ca_3(PO_4)_2$-like phases (1), Fe_2P (2), FeP (3), and β-$Ca_2P_2O_7$ (4) are indicated by tick marks.

(25) Wappling, R.; Haggstrom, L.; Rundqvist, S.; Karlsson, E. *J. Solid State Chem.* **1971**, *3*, 276.

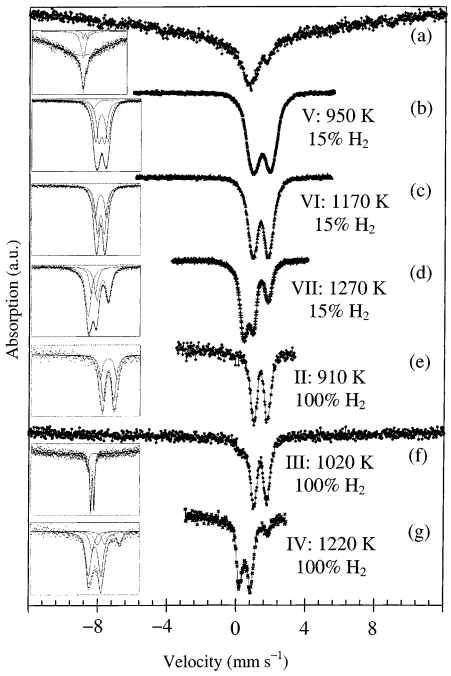

Figure 3. Mössbauer spectra (source: ^{57}Co/Cr) at RT of s-$Ca_9Fe(PO_4)_7$ (a), samples V (b), VI (c), and VII (d) (see text), and samples II (e), III (f), and IV (g) (see Figure 1). Insets present decompositions of the spectra. The spectra a−d were obtained using samples with 14% ^{57}Fe; the spectra e−g were obtained using samples with the natural content of ^{57}Fe.

Because the gas phase was not analyzed, we do not specify its composition.

From the experimental loss in mass of ca. 5.6% (Figure 1) for sample IV, we could obtain the amount of O and P atoms lost by the sample. The calculated loss in mass based on eq 3 is 5.7%. XRD proved sample IV to contain FeP (ICDD PDF #71-2262) and Fe_2P (ICDD PDF #83-2337) in addition to a β-$Ca_3(PO_4)_2$-like phase (Figure 2e). Mass fractions of FeP and Fe_2P obtained from the XRD data were 4.6% and 1.3%, respectively. We used these experimental results to estimate the coefficients before FeP and Fe_2P in eq 3. The calculated mass fractions according to eq 3 are ca. 4.7% for FeP and ca. 1.7% for Fe_2P. Mössbauer spectroscopy also confirmed the presence of iron phosphides[25] in sample IV (Figure 3g) and indicated that ca. 17% of Fe atoms in sample IV had the oxidation state of +2 and parameters ($\delta \approx 1.25$ mm/s and $\Delta E_Q \approx 0.81$ mm/s) close to those of Fe^{2+} ions in β-$Ca_3(PO_4)_2$-like phases (Table 1). Using this fact, we assumed the composition of the β-$Ca_3(PO_4)_2$-like phase to be $Ca_{2.935}Fe^{2+}_{0.065}(PO_4)_2$. With eq 3, the calculated fraction of Fe atoms located in the β-$Ca_3(PO_4)_2$-like phase is 20%. In addition, lattice parameters of $Ca_{2.935}Fe^{2+}_{0.065}(PO_4)_2$ (a = 10.4259(8) Å and c = 37.327(3) Å) were a little less than those of β-$Ca_3(PO_4)_2$ (a = 10.439 Å and c = 37.375 Å; Figure 2g),[15] but much larger than those of $Ca_9FeH(PO_4)_7$ (a = 10.3689 Å and c = 37.128 Å). It is consistent with the small amount of Fe^{2+} ions in $Ca_{2.935}Fe^{2+}_{0.065}(PO_4)_2$, which is a member of solid solutions $Ca_{3-x}Fe_x(PO_4)_2$ with x = 0.065. Solid solutions $Ca_{3-x}Fe_x(PO_4)_2$ are formed in a compositional range of $0 \le x \le 0.33$.[26]

(26) Nord, A. G. *Neues Jahrb. Mineral., Monatsh.* **1983**, *11*, 489.

Table 1. Parameters of Mössbauer Spectra (Numbers in Parentheses Are Estimated Standard Deviations of the Last Significant Digits)

sample	δ^a (mm s^{-1})	$\Delta E_Q{}^b$ (mm s^{-1})	Γ^c (mm s^{-1})	S^d (%)
s-$Ca_9Fe(PO_4)_7$	0.20(5)		17.9(9)	90(2)
	0.58(2)		1.55(7)	8(2)
	1.10(2)	1.07(2)	0.48(9)	2(2)
V: reduced at 950 K for 20 h in 15% H_2 + 85% Ar	1.28(1)	1.29(1)	0.61(1)^e	50(1)
	1.29(1)	0.61(1)	0.61^e	45(1)
	0.43(1)		0.61^e	5(1)
VI: reduced at 1170 K for 20 h in 15% H_2 + 85% Ar	1.20(1)	1.20(1)	0.51(1)^f	42(1)
	1.20(1)	0.72(1)	0.51^f	58(1)
VII: reduced at 1270 K for 20 h in 15% H_2 + 85% Ar	1.24(1)	0.83(1)	0.43(1)	41(1)
	0.19(1)		0.48(1)	35(1)
	0.56(1)	0.31(1)	0.39(1)	24(1)
II: heated to 910 K in 100% H_2	1.20(1)	1.07(1)	0.32(1)^g	36(1)
	1.20(1)	0.68(1)	0.32^g	64(1)
III: heated to 1020 K in 100% H_2	1.23(1)	0.76(1)	0.43(1)	87(1)
	0.13(1)	0.37(1)	0.50(1)	13(1)
IV: heated to 1220 K in 100% H_2	1.25(1)	0.81(1)	0.32(1)^h	17(1)
	0.33(1)	0.68(1)	0.32^h	59(1)
	0.19(1)	-	0.32^h	13(1)
	0.47(1)	0.16(1)	0.32^h	11(1)
$Ca_9FeH_{0.85}(PO_4)_7$ T = 750 K for 43 h in 15% H_2 + 85% Ar	1.22(1)	1.00(1)	0.34(1)	44(1)
	1.21(1)	0.66(1)	0.28(1)	41(1)
	0.26(1)	0.68(1)	0.50(1)	15(1)
$Ca_9FeH(PO_4)_7$, T = 800 K for 45 h in 15% H_2 + 85% Ar	1.26(1)	1.00(1)	0.27(1)^i	42(1)
	1.26(1)	0.65(1)	0.27^i	58(1)

^{a} Isomer shift. ^{b} Quadrupole splitting. ^{c} Full-width at half-maximum. ^{d} Relative spectral area. ^{e} −^{i}These Γ values were constrained to be equal to each other.

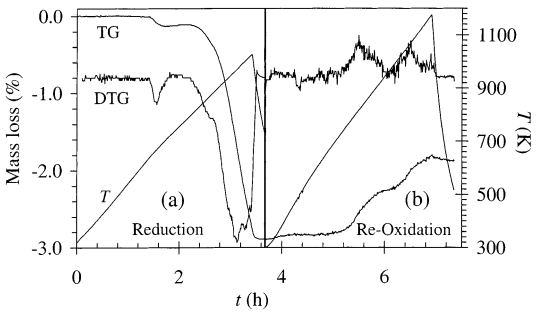

Figure 4. T, TG, and DTG versus time (t) curves of (a) heating of s-$Ca_9Fe(PO_4)_7$ in 100% H_2 from RT to 1020 K (sample III) and (b) subsequent re-oxidation of sample III in air.

To fulfill all the experimental facts, we needed to assign noninteger stoichiometric coefficients in eq 3. The origin for that is a variable amount-of-substance ratio between FeP and Fe_2P and a variable x value in solid solutions $Ca_{3-x}Fe_x(PO_4)_2$. Appearance of Fe_2P is ascribable in terms of decomposition of FeP at high temperatures to form Fe_2P.[27]

Re-oxidation of sample IV in air at 1270 K yielded a bright-red mixture consisting of α-Fe_2O_3 (ca. 2.2%) and two β-$Ca_3(PO_4)_2$-like phases with lattice parameters of a = 10.3419(11) Å and c = 37.165(5) Å (ca. 48.8%) and a = 10.3987(11) Å and c = 37.287(5) Å (ca. 49.0%).

(27) Brauer, G. *The Guidance on Inorganic Synthesis* (in Russian); Mir: Moscow, 1985.

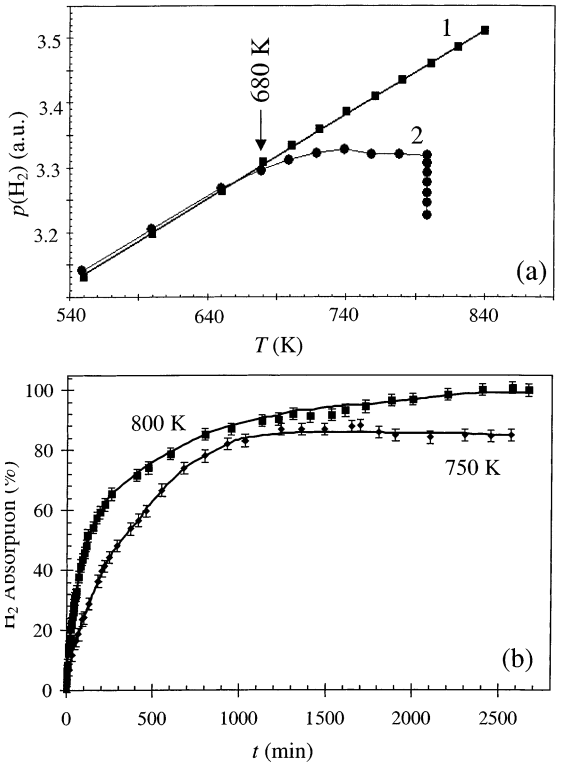

Figure 5. H_2 absorption curves by s-$Ca_9Fe(PO_4)_7$. (a) Temperature dependence of H_2 pressure, $p(H_2)$, in the reactor without samples (1) and with s-$Ca_9Fe(PO_4)_7$ (2). (b) H_2 absorption curves at different temperatures. Initial concentration of H_2 was 15%.

A long treatment (3−5 h) of s-$Ca_9Fe(PO_4)_7$ in 100% H_2 at 1220 K led to formation of only one phosphide, Fe_2P, in addition to a β-$Ca_3(PO_4)_2$-like phase. This fact gave evidence that an ideal reaction at 1220 K in 100% H_2 can be presented as

$$2Ca_9Fe(PO_4)_7 \xrightarrow{H_2} 6Ca_3(PO_4)_2 + Fe_2P + \text{“P} + 8H_2O\text{”}\uparrow \quad (4)$$

when it is complete.

Figure 5a presents temperature dependence of $p(H_2)$ in the setup when the reactor did not contain and contained s-$Ca_9Fe(PO_4)_7$. The $p(H_2)$ versus T curve was linear when the reactor was without samples. Deviation from the linear dependence at ca. 680 K, when s-$Ca_9Fe(PO_4)_7$ was placed in the reactor, showed that H_2 pressure reduced in the setup and, therefore, $Ca_9Fe(PO_4)_7$ started to absorb hydrogen atoms. In other words, this fact indicated the onset of a reduction process above 680 K, that is, introduction of H^+ ions in the structure to form $Ca_9FeH_x(PO_4)_7$ (see eq 1).

Samples reduced in 100% H_2 at temperatures below 680 K were light red and their Mössbauer spectra and XRD patterns were very close to those of s-$Ca_9Fe(PO_4)_7$.[8,17] Mössbauer spectra of these samples consisted of a broad and diffuse peak (Figure 3a and Table 1). Samples reduced in the temperature range from 680 to 820 K were pink-white or white depending on reduction time. They were monophasic. These findings together with the results of the TG measurements confirmed that, in the temperature range of 680 to 820 K, the fundamental structure of $Ca_9FeH_x(PO_4)_7$ is not destroyed in redox reactions.

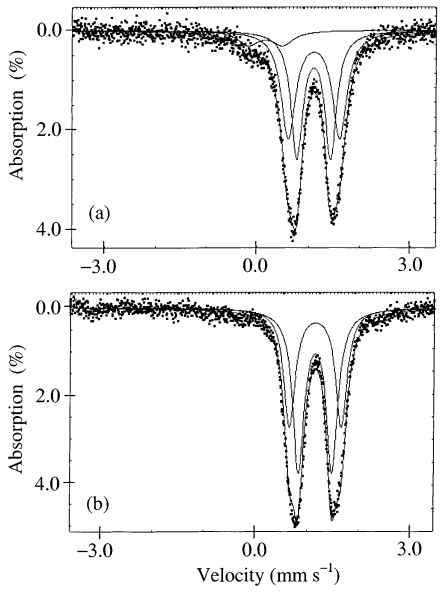

Figure 6. Mössbauer spectra of (a) $Ca_9FeH_{0.85}(PO_4)_7$ and (b) $Ca_9FeH(PO_4)_7$ at RT (source: $^{57}Co/Rh$; the natural content of ^{57}Fe).

Reduction of $Ca_9Fe(PO_4)_7$ at Low H_2 Concentrations. H_2 absorption curves were measured below 820 K, that is, when the structure of $Ca_9FeH_x(PO_4)_7$ was stable. Figure 5b displays the dependence of the quantity of absorbed H_2 (in % from the complete reduction of Fe^{3+} to Fe^{2+}) on time at two different temperatures, 750 and 800 K. This figure shows that ca. 85% of H atoms was absorbed at 750 K, and ca. 100% at 800 K. The composition of the obtained samples can, therefore, be presented as $Ca_9Fe^{3+}_{0.15}Fe^{2+}_{0.85}H_{0.85}(PO_4)_7$ (a = 10.3623(5) Å and c = 37.126(2) Å) and $Ca_9Fe^{2+}H(PO_4)_7$ (a = 10.3689(5) Å and c = 37.128(2) Å), respectively. The higher the temperature of reduction, the more quantity of H^+ ions entered into the structure.

Mössbauer spectroscopy confirmed the oxidation state of Fe atoms in $Ca_9FeH_{0.85}(PO_4)_7$ and $Ca_9FeH(PO_4)_7$ and, therefore, the content of H^+ ions. The Mössbauer spectrum of $Ca_9FeH(PO_4)_7$ was very close to that given in the literature[8,18,22] and consisted of two doublets with $\delta \approx 1.26$ mm/s (Figure 6b, Table 1) characteristic of Fe^{2+} ions. The Mössbauer spectrum of $Ca_9FeH_{0.85}(PO_4)_7$ (Figure 6a, Table 1) showed the presence of ca. 15% of Fe^{3+} ions (with $\delta \approx 0.26$ mm/s) in addition to Fe^{2+} ions (ca. 85% with $\delta \approx 1.21$ mm/s).

The presence of components corresponding to Fe^{3+} ions in Mössbauer spectra may be caused by either “over-reduction” with partial destruction of the structure and appearance of iron phosphides as for sample III (Figure 3f) or partial reduction of Fe^{3+} to Fe^{2+} to form $Ca_9FeH_x(PO_4)_7$ ($0 < x < 1$) with maintaining the structure as for $Ca_9FeH_{0.85}(PO_4)_7$ (Figure 6a).

The Mössbauer spectra of s-$Ca_9Fe(PO_4)_7$ reduced in 15% H_2 + 85% Ar for 20 h at 950 K (sample V) and 1170 K (sample VI) (Figure 3b,c) were very close to that of $Ca_9FeH(PO_4)_7$[8,18,22] and also had two doublets with $\delta \approx 1.20$ mm/s. Samples V and VI were white. XRD showed sample V to contain only a β-$Ca_3(PO_4)_2$-like phase whereas sample VI consisted of a β-$Ca_3(PO_4)_2$-like phase and β-$Ca_2P_2O_7$ (Figure 2f). Appearance of β-$Ca_2P_2O_7$ was caused by thermal decomposition of $Ca_9FeH_x(PO_4)_7$. The decomposition reaction proceeded with

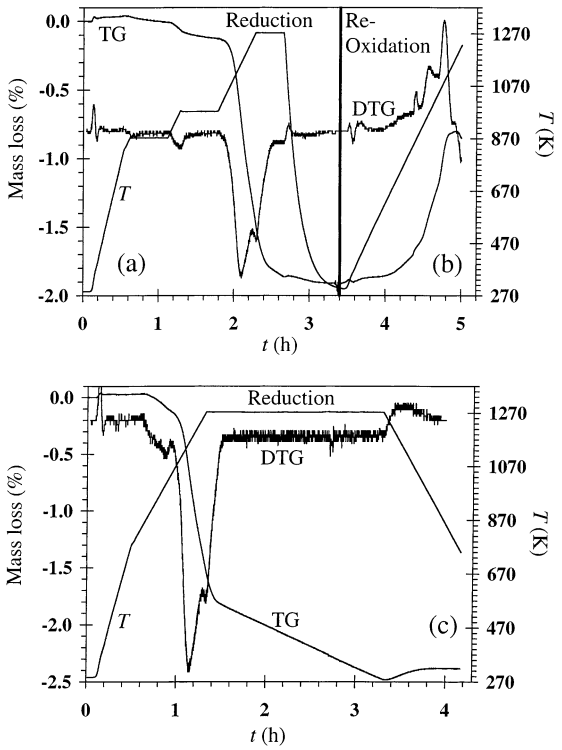

Figure 7. *T*, TG, and DTG versus time (*t*) curves for (a, c) treatment of s-$Ca_9Fe(PO_4)_7$ in 5% H_2 + 95% N_2 and (b) subsequent re-oxidation in air.

keeping the oxidation state of Fe and releasing H_2O is expressed by the following reaction:[22]

$$14Ca_9Fe^{2+}H(PO_4)_7 = 7Ca_2P_2O_7 + 12Ca_{9.333}Fe^{2+}{}_{1.167}(PO_4)_7 + 7H_2O \quad (5)$$

Note that sample VI was white and had Fe atoms in an oxidation state of +2 (Figure 3c) in contrast to sample III which was dark gray and probably contained amorphous FeP (Figure 3f).

The Mössbauer spectrum of s-$Ca_9Fe(PO_4)_7$ treated in 15% H_2 + 85% Ar at 1270 K for 20 h (sample VII) showed the presence of components with $\delta \approx 1.24$ mm/s (Fe^{2+} ions in a β-$Ca_3(PO_4)_2$-like phase) and $\delta \approx 0.19$ and 0.56 mm/s, which may be assigned to Fe_2P (Figure 3d).[25] The presence of Fe_2P as well as a β-$Ca_3(PO_4)_2$-like phase in sample VII was confirmed by XRD. Note that β-$Ca_2P_2O_7$ was not found in sample VII.

Figure 7 shows the TG curves of s-$Ca_9Fe(PO_4)_7$ in 5% H_2 + 95% N_2. The reduction process at low H_2 concentration obviously differed from reduction in 100% H_2. Loss in mass observed above ca. 870 K was probably caused by the thermal decomposition of partially reduced phases, $Ca_9FeH_x(PO_4)_7$, by analogue with eq 5.[22]

Sharp loss in mass of ca. 1.8% was observed from 1020 to 1270 K. Annealing at 1270 K led to loss in mass with a constant rate (Figure 7c). A two-step decomposition process could be seen from the differential TG (DTG) curves in the temperature range from 1020 to 1270 K with the maxima on the DTG curves at 1140 and 1260 K. These two processes could be separated by annealing at 1170 K followed by annealing at 1270 K.

s-$Ca_9Fe(PO_4)_7$ reduced at 1270 K in 5% H_2 + 95% N_2 (Figure 7a) was dark gray. An increase in mass of ca. 1.1% during re-oxidation of this sample (Figure 7b) was less than the loss in mass of ca. 1.9% during reduction due to changing the content of P atoms.

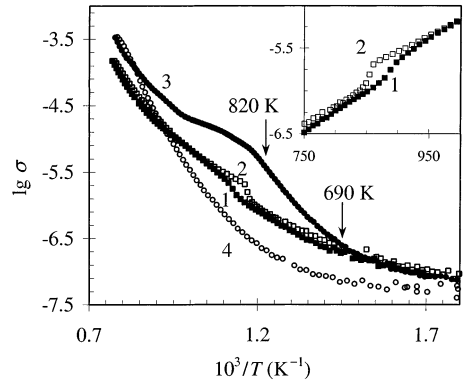

Figure 8. Plot of lg σ versus T^{-1} for s-$Ca_9Fe(PO_4)_7$ under (1, 2) air and (3, 4) a reduction atmosphere, 5% H_2 + 95% N_2, during (1, 3) heating and (2, 4) cooling. Unit of σ: S·cm^{-1}; lg σ = log σ. Inset shows the lg σ versus *T* curve in the vicinity of the phase transition.

Figure 8 presents temperature dependence of electrical conductivities of s-$Ca_9Fe(PO_4)_7$ in air and 5% H_2 + 95% N_2. Differences in conductivities under air and 5% H_2 + 95% N_2 were observed from ca. 690 K (Figure 8, curve 3). This temperature agrees well with the temperature of the onset of the reduction process (see eq 1) found in the H_2 absorption experiments (Figure 5a). Electrical conductivities in air and 5% H_2 + 95% N_2 differed by a factor of ca. 6 at 820 K. Under the 5% H_2 + 95% N_2 atmosphere, the lg σ versus T^{-1} curves during heating and cooling did not coincide with each other because decomposition reactions took place above 820−870 K (see eqs 3−5). In air, these curves were very similar to each other during heating and cooling. Small jumps with temperature hysteresis at ca. 870 K on the lg σ versus T^{-1} curves of s-$Ca_9Fe(PO_4)_7$ in air were caused by the first-order ferroelectric phase transition in $Ca_9Fe(PO_4)_7$ with the phase transition temperature of 890 K.[28]

Magnetic Properties of s-$Ca_9Fe(PO_4)_7$ and Reduced Samples. A plot of $(\chi - \chi_0)^{-1}$ against temperature, *T*, for s-$Ca_9Fe(PO_4)_7$ (Figure 9) obeyed the modified Curie−Weiss rule in the whole temperature range, 300−1000 K,

$$(\chi - \chi_0)^{-1} = (T - \theta)/C \quad (6)$$

where χ_0 (= -3.32×10^{-4} cm^3 mol^{-1}) is the temperature-independent term including a diamagnetic constituent and Van Fleka paramagnetism, *C* (=4.485 cm^3 K mol^{-1}) is the Curie constant, and (θ = −9.5 K) is the Weiss constant. The effective magnetic moment, $\mu_e = (8C)^{1/2}$, was calculated at 5.99 μ_B (μ_B: Bohr magneton) per Fe^{3+} ion. This value is close to a theoretical one, 5.92 μ_B, expected for the free Fe^{3+} ion in the high-spin configuration.[29] The small negative Weiss constant indicates the presence of very weak antiferromagnetic coupling between the Fe^{3+} ions. Nonlinear behavior of the (χ −

(28) Lazoryak, B. I.; Morozov, V. A.; Belik, A. A.; Stefanovich, S. Yu.; Grebenev, V. V.; Leonidov, I. A.; Mitberg, E. B.; Davydov, S. A.; Lebedev, O. I.; Van Tendeloo, G. Submitted for publication to *Solid State Sci.*

(29) Kittel, C. *Introduction to Solid State Physics, 7th ed.*; John Wiley: New York, 1996.

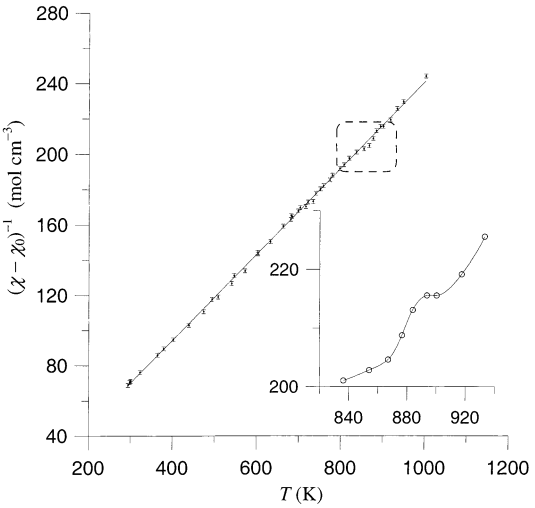

Figure 9. Plot of inverse magnetic susceptibility, $(\chi - \chi_0)^{-1}$, versus temperature, T, for s-$Ca_9Fe(PO_4)_7$. Inset shows a fragment from 840 to 940 K.

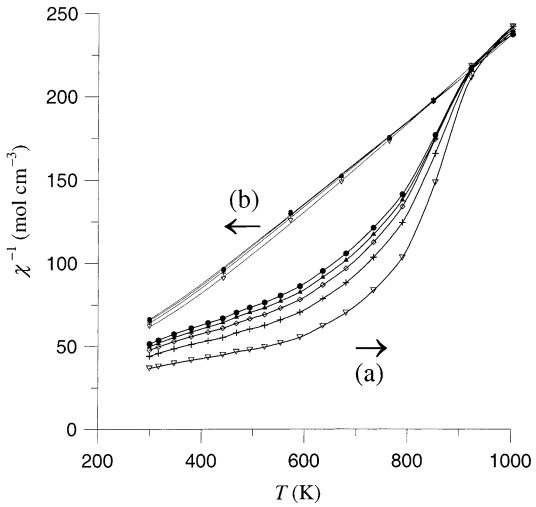

Figure 10. Plot of inverse magnetic susceptibility, χ^{-1}, versus temperature, T, during (a) heating and (b) cooling under air for $Ca_9FeH(PO_4)_7$ in an applied magnetic field, H, of 5950 Oe (▽), 9763 Oe (+), 12045 Oe (◇), 13522 Oe (▲), and 14779 Oe (●).

$\chi_0)^{-1}$ versus T curve from 860 to 920 K (Figure 9) was caused by the ferroelectric phase transition in $Ca_9Fe(PO_4)_7$.[28]

Magnetic susceptibilities of $Ca_9FeH(PO_4)_7$ strongly depended on an attached magnetic field (Figure 10). Such behavior usually indicates the presence of ferromagnetic impurities. Ferromagnetic impurities in paramagnetic $Ca_9FeH(PO_4)_7$ masked weak effects connected with the presence of Fe^{2+} ions in $Ca_9FeH(PO_4)_7$. For this reason, we do not give fitting parameters and results. The possible ferromagnetic impurity in $Ca_9FeH(PO_4)_7$ is metal iron because s-$Ca_9Fe(PO_4)_7$ contained impurity of Fe_2O_3.

After oxidation of $Ca_9FeH(PO_4)_7$ in air, the dependence of χ^{-1} on an attached magnetic field almost disappeared (Figure 10b). The resultant χ^{-1} versus T curves coincided with that for s-$Ca_9Fe(PO_4)_7$ (Figure 9). Independence of χ^{-1} from the attached magnetic field for s-$Ca_9Fe(PO_4)_7$ and oxidized samples indicated that they did not contain ferromagnetic impurities. Metal iron in $Ca_9FeH(PO_4)_7$ transformed to Fe_2O_3 in the oxidized samples. A small amount of antiferromagnetic Fe_2O_3 has no influence on the magnetic moment of Fe atoms in $Ca_9Fe(PO_4)_7$.

In this work, we have studied behavior of $Ca_9Fe(PO_4)_7$ in a reduction atmosphere as a function of temperature and H_2 concentration. Above 820−870 K in a reduction atmosphere, the fundamental structure of $Ca_9FeH_x(PO_4)_7$ starts to destroy with formation of FeP (Fe_2P) or β-$Ca_2P_2O_7$ depending on H_2 concentration. In the temperature range of 680−820 K, the redox reactions proceed reversibly. The experimental data obtained are important for potential applications of $Ca_9Fe(PO_4)_7$ as a catalyst, a material for cleaning gas mixtures from H_2, and a material intermediator for two-stage oxidation of H_2.

Acknowledgment. This work was supported by the Russian Foundation for Basic Research (Grants 00-03-32660 and 01-03-06122). The authors thank S. S. Khasanov of the Institute of Solid State Physics for his help in the XRD experiments and K. V. Pokholok and M. I. Afanasov of Moscow State University for the measurements of the Mössbauer spectra.

Note Added after ASAP Posting. This article was posted ASAP on 1/11/2003 with an error in the manuscript received date. The correct version was posted on 1/30/2003.

CM010851L